Structural changes of region 1-16 of the Alzheimer disease amyloid beta-peptide upon zinc binding and in vitro aging.

Séverine Zirah, Sergey A Kozin, Alexey K Mazur, Alain Blond, Michel Cheminant, Isabelle Ségalas-Milazzo, Pascale Debey, Sylvie Rebuffat

THE JOURNAL OF BIOLOGICAL CHEMISTRY VOL. 281, NO. 4, pp. 2151–2161, January 27, 2006

Structural Changes of Region 1–16 of the Alzheimer Disease Amyloid β-Peptide upon Zinc Binding and *in Vitro* Aging*[S]

Received for publication, April 25, 2005, and in revised form, October 26, 2005 Published, JBC Papers in Press, November 21, 2005, DOI 10.1074/jbc.M504454200

Séverine Zirah[‡1], Sergey A. Kozin[‡§1], Alexey K. Mazur[¶], Alain Blond[‡], Michel Cheminant[‡], Isabelle Ségalas-Milazzo[‖], Pascale Debey[**], and Sylvie Rebuffat[‡2]

From the [‡]Laboratoire de Chimie et Biochimie des Substances Naturelles, UMR 5154 CNRS-MNHN, Département Régulations, Développement et Diversité Moléculaire, Muséum National d'Histoire Naturelle, 63 Rue Buffon, 75005 Paris, France, [¶]UPR 9080 CNRS, Institut de Biologie Physico-Chimique, 13 Rue Pierre et Marie Curie, 75005 Paris, France, the [‖]Laboratoire de RMN, IRCOF, UMR 6014 CNRS, IFRMP 23, Université de Rouen, Mont-Saint-Aignan, France, the [**]Laboratoire de Régulation et Dynamique des Génomes, UMR 5153 CNRS-MNHN, U565 INSERM, Département Régulations, Développement et Diversité Moléculaire, Muséum National d'Histoire Naturelle, 43 Rue Cuvier, 75005 Paris, France, and the [§]Proteomics Department, Institute of Biomedical Chemistry RAMS, 10 Pogodinskaya Street, Moscow 119121, Russia

Amyloid deposits within the cerebral tissue constitute a characteristic lesion associated with Alzheimer disease. They mainly consist of the amyloid peptide Aβ and display an abnormal content in Zn^{2+} ions, together with many truncated, isomerized, and racemized forms of Aβ. The region 1–16 of Aβ can be considered the minimal zinc-binding domain and contains two aspartates subject to protein aging. The influence of zinc binding and protein aging related modifications on the conformation of this region of Aβ is of importance given the potentiality of this domain to constitute a therapeutic target, especially for immunization approaches. In this study, we determined from NMR data the solution structure of the Aβ-(1–16)-Zn^{2+} complex in aqueous solution at pH 6.5. The residues His^6, His^{13}, and His^{14} and the Glu^{11} carboxylate were identified as ligands that tetrahedrally coordinate the Zn(II) cation. *In vitro* aging experiments on Aβ-(1–16) led to the formation of truncated and isomerized species. The major isomer generated, Aβ-(1–16)-L-iso-Asp^7, displayed a local conformational change in the His^6–Ser^8 region but kept a zinc binding propensity via a coordination mode involving L-iso-Asp^7. These results are discussed here with regard to Aβ fibrillogenesis and the potentiality of the region 1–16 of Aβ to be used as a therapeutic target.

Amyloid deposition in senile plaques is one of the main cerebral damages associated with Alzheimer disease (AD).[3] The amyloid β-peptide (Aβ), the major component of these extracellular deposits, is a 39–43-amino acid peptide that results from the normal proteolytic processing of the amyloid precursor protein.

Considerable NMR data obtained on Aβ and on fragments argue that the soluble monomeric peptide is in an unordered conformation in aqueous solution and mainly adopts an α-helical structure in membrane-mimicking media (1–9). By contrast, the conformation of Aβ within amyloid fibrils consists mainly of a β-sheet structure (10–12). Therefore, as for other conformational diseases (13), a transconformation toward β-sheet is assumed to trigger the abnormal fibrillar amyloid deposition associated with AD. The N-terminal region of Aβ has been shown to be flexible and accessible within amyloid fibrils (14, 15). Therefore, it constitutes an attractive therapeutic target, as illustrated by the ability of monoclonal antibodies directed toward this region to dissociate amyloid fibrils (16, 17).

Imbalances in transition metal cations such as copper, zinc, and iron are assumed to contribute to Aβ deposition (18). In particular, (i) Zn^{2+} ions have been shown to trigger Aβ aggregation (19–21), and (ii) abnormally high levels of zinc have been found within amyloid deposits in AD patients (22, 23). However, the role of zinc in amyloid deposition is subject to debate (24, 25) as (i) Zn^{2+} ions induce the deposition of Aβ in the form of nonfibrillar aggregates (26, 27), and (ii) zinc has been shown to function as an antioxidant able to protect from extensive redox chemical reactions that contribute to AD-related oxidative stress (28, 29). The obligatory sequence involved in zinc binding has been mapped to the region 6–28 of Aβ (30), and the involvement of the His^{13} and His^{14} residues has been strongly suggested (31–33). Because of marked aggregation of Aβ peptides or Aβ fragments in the presence of Zn^{2+}, zinc-induced conformational switching has not yet been characterized. However, using Aβ-(1–16), a synthetic peptide spanning the amino acid sequence between the α- and β-secretase cleavage sites, we showed in our initial CD study that this fragment of Aβ selectively bound Zn^{2+} to form a 1:1 complex soluble in physiologically relevant conditions and subsequently underwent a conformational change (34). We proposed a model of zinc attachment that involved the three histidines, His^6, His^{13}, and His^{14}, and hypothesized Arg^5 as the fourth coordination ligand from the analysis of the Aβ-(1–16)-Zn^{2+} 1:1 complex in the gas phase by electrospray-ionization mass spectrometry (ESI-MS) (35). Recently, the zinc binding property of Aβ-(1–16) was studied by Mekmouche *et al.* (36), and the apparent dissociation constant of the 1:1 complex was determined.

In addition to its zinc binding propensity, the 1–16 N-terminal region of Aβ is subject to isomerization and racemization of the aspartate residues, which constitute very common types of aging-related protein

* The costs of publication of this article were defrayed in part by the payment of page charges. This article must therefore be hereby marked "*advertisement*" in accordance with 18 U.S.C. Section 1734 solely to indicate this fact.

The atomic coordinates and structure factors (code 1ZE7, 1ZE9, and 2BP4) have been deposited in the Protein Data Bank, Research Collaboratory for Structural Bioinformatics, Rutgers University, New Brunswick, NJ (http://www.rcsb.org/).

[S] The on-line version of this article (available at http://www.jbc.org) contains Fig. S1 and Tables A and B.

[1] Both authors contributed equally to this work.

[2] To whom correspondence should be addressed: Département Régulations, Développement et Diversité Moléculaire, UMR 5154 CNRS-MNHN, Muséum National d'Histoire Naturelle, Case postale 54, 57 Rue Cuvier, 75005 Paris, France. Tel.: 33-1-40-79-31-18; Fax: 33-1-40-79-31-35; E-mail: rebuffat@mnhn.fr.

[3] The abbreviations used are: AD, Alzheimer disease; ACN, acetonitrile; Aβ, amyloid β-peptide; Aβ-(1–16), 1–16 N-terminal region of Aβ; CSD, chemical shift deviations; DQF-COSY, double quantum filtered correlation spectroscopy; ESI, electrospray ionization; GC, gas chromatography; HMBC, heteronuclear multiple bond correlation; HSQC, heteronuclear single quantum correlation; MS, mass spectrometry; NOE, nuclear Overhauser effect; NOESY, nuclear Overhauser effect spectroscopy; RP-HPLC, reversed phase-high performance liquid chromatography; TOCSY, total correlation spectroscopy.

damages. These chemical modifications occur through a common pathway involving a neutral cyclic succinimide intermediate (37, 38). The potential contribution of such aspartyl modifications to Aβ amyloidosis has been addressed, because unusually high contents of racemized and isomerized Asp residues were found in Aβ isolated from amyloid deposits (39). In addition, these modifications were shown to be related to an increase in β-sheet content and to *in vitro* fibrillation (40, 41), leading to the protein aging hypothesis of AD (42). On the other hand, the assessment of plaque age by using antibodies targeting specifically a particular isomer of Aβ suggests that these modifications would occur rather after the amyloid deposition (43).

The N-terminal region of Aβ appears as an attractive therapeutic target, especially for active or passive immunization approaches. Indeed, only the antibodies raised against the N-terminal part of Aβ are able to reduce the plaque burden and restore cognitive deficits in the mice model of AD (16, 44, 45). In addition, targeting this region should enable us to exert this effect without eliciting an inflammatory response, which had been critical in the first clinical tests of active immunization on humans (46). We have shown previously that Aβ-(1–16) zinc binding induces an agonist effect on the 4–10 epitope recognition by different monoclonal antibodies, suggesting a folding of the peptide that would render the epitope more accessible (47). Because clinical testing for passive immunization has started, it is of major importance to characterize the structural changes of the N-terminal region of Aβ upon zinc binding and protein aging-induced modifications.

Here we used NMR and molecular modeling to determine the three-dimensional structure of the apoAβ-(1–16) and the Aβ-(1–16)-Zn^{2+} complex in aqueous solution at pH 6.5. Furthermore, we investigated the ability of Aβ-(1–16) to undergo protein aging-related modifications. *In vitro* aging experiments were performed on the synthetic peptide Aβ-(1–16) in the absence and in the presence of Zn^{2+} ions. The resultant species were isolated and identified, and the main isomers generated were analyzed by NMR. From our study, region 1–16 of Aβ would behave as an autonomous segment able to undergo both zinc binding-induced structuration and aging-related isomerizations.

EXPERIMENTAL PROCEDURES

Synthetic Peptides—The synthetic peptides used throughout this study were purchased from Eurogentec (Angers, France) with a ≥95% purity checked by RP-HPLC and matrix-assisted desorption ionization time-of-flight mass spectrometry (Voyager-DEPro, Applied Biosystems, Courtaboeuf, France). Aβ-(1–16) (Ac-Asp-Ala-Glu-Phe-Arg^5-His-Asp-Ser-Gly-Tyr^{10}-Glu-Val-His-His-Glu^{15}-Lys-NH_2) was acetylated at the N terminus and amidated at the C terminus; $Aβ\text{-}(1–16)^{hemi}$ was nonacetylated at the N terminus and amidated at the C terminus; Aβ-(1–16)-L-iso-Asp^7 was acetylated at the N terminus and amidated at the C terminus and contained one L-iso-Asp residue at position 7.

NMR Spectroscopy—Aβ-(1–16) was dissolved either in 50 mM sodium phosphate buffer, pH 6.5, or in Tris-d_{11}/HCl 22.5 mM, pH 5.8, prepared in H_2O/D_2O (9:1) using MilliQ™ water samples (Millipore, Saint-Quentin-en-Yvelines, France). The pH was checked directly in the 5-mm Wilmad NMR tubes by using a Mettler Toledo U402-M3-S7/200 electrode. pH values were uncorrected for deuterium isotope effects. Samples for experiments in the presence of Zn^{2+} were prepared by adding a concentrated stock solution of the highest analytical grade $ZnCl_2$ (Aldrich) in order to reach a Zn^{2+}/peptide ratio of 1.5. The absence of pH variation upon zinc addition was checked. Alternatively, Aβ-(1–16) and Aβ-(1–16)-L-iso-Asp^7 were analyzed at 3 mM in 50 mM sodium phosphate buffer, pH 7.5, prepared in H_2O/D_2O (9:1).

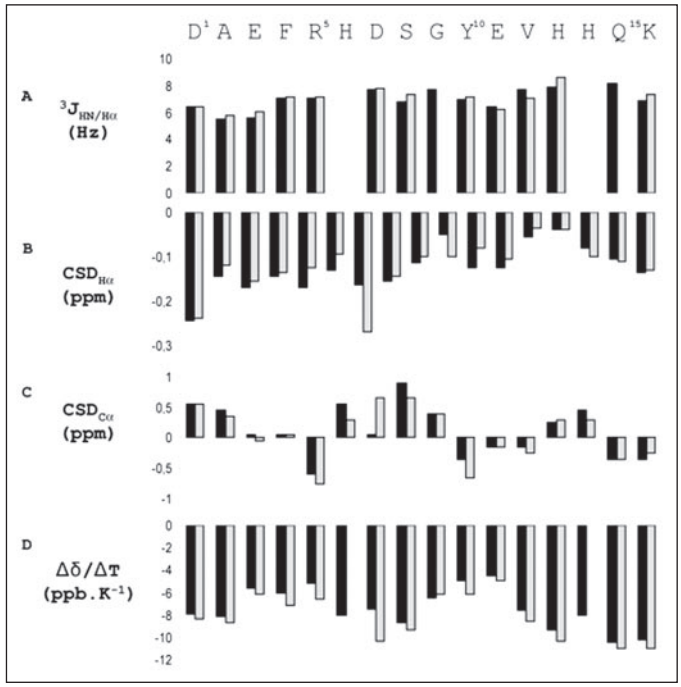

FIGURE 1. **Conformational parameters for Aβ-(1–16) (*black*) and Aβ-(1–16)-L-iso-Asp^7 (*gray*) at pH 7. 4.** *A*, $^3J_{HN\text{-}H\alpha}$ coupling constants. *B* and *C*, chemical shift deviations calculated for the H-α and C-α according to Refs. 48 and 49. *D*, Δδ/Δ*T* coefficients determined for the amide protons.

NMR experiments were carried out on AVANCE 400 and DMX 600 spectrometers (Bruker Biospin, Wissembourg, France) both equipped with shielded gradients *z* and set up with ^1H broad band reverse gradient and triple resonance ^1H-^{13}C-^{15}N gradient probe heads, respectively. Temperature was controlled with a BCU-05 refrigeration unit and a BVT 3000 control unit on both spectrometers. ^1H and ^{13}C chemical shifts were externally referenced to sodium 2,2-dimethyl-2-silapentane-5-sulfonate. Conventional one- and two-dimensional experiments, one-dimensional ^1H, ^1H-^1H DQF-COSY, TOCSY (using a spin-lock field produced by an MLEV-17 spin-locking sequence for a spin-lock time of 120 ms), NOESY (with mixing times of 100, 200, 300, and 400 ms), as well as natural abundance ^1H-^{13}C HSQC and HMBC (with long-range coupling evolution delays of 70 ms and 90 ms) were performed. Water suppression was achieved by means of either selective low power irradiation for the DQF-COSY experiment or pulsed field gradients in a water suppression by a gradient tailored excitation scheme included in the pulse sequences for both TOCSY and NOESY experiments. Data were processed on Silicon Graphics Indigo 2 XL or O_2 workstations, using XWINNMR 3.1 and AURELIA software (Bruker Biospin, Wissembourg, France).

The determination of temperature coefficients ($\Delta\delta/\Delta T_{HN}$) was achieved for each sample from five series of ^1H one-dimensional and TOCSY spectra recorded between 288 and 313 K. $^3J_{HN\text{-}H\alpha}$ coupling constants were determined from ^1H one-dimensional and DQF-COSY spectra. The chemical shift deviations (CSD) were calculated for H-α and C-α atoms considering the reference chemical shifts proposed by Wishart *et al.* (48, 49) for each amino acid in random structure.

The pK_a values of the histidines were measured in the absence of Zn^{2+} ions by using 3.5 mM Aβ-(1–16) peptide solutions in 10 mM H_2O/D_2O (9:1) sodium phosphate buffer. The effects of pH on the proton chemical shifts of Aβ-(1–16) were determined from a series of ^1H one-dimensional, TOCSY, and NOESY spectra recorded at different pH values ranging from 3.0 to 9.5 at 278 K. The pH values were adjusted

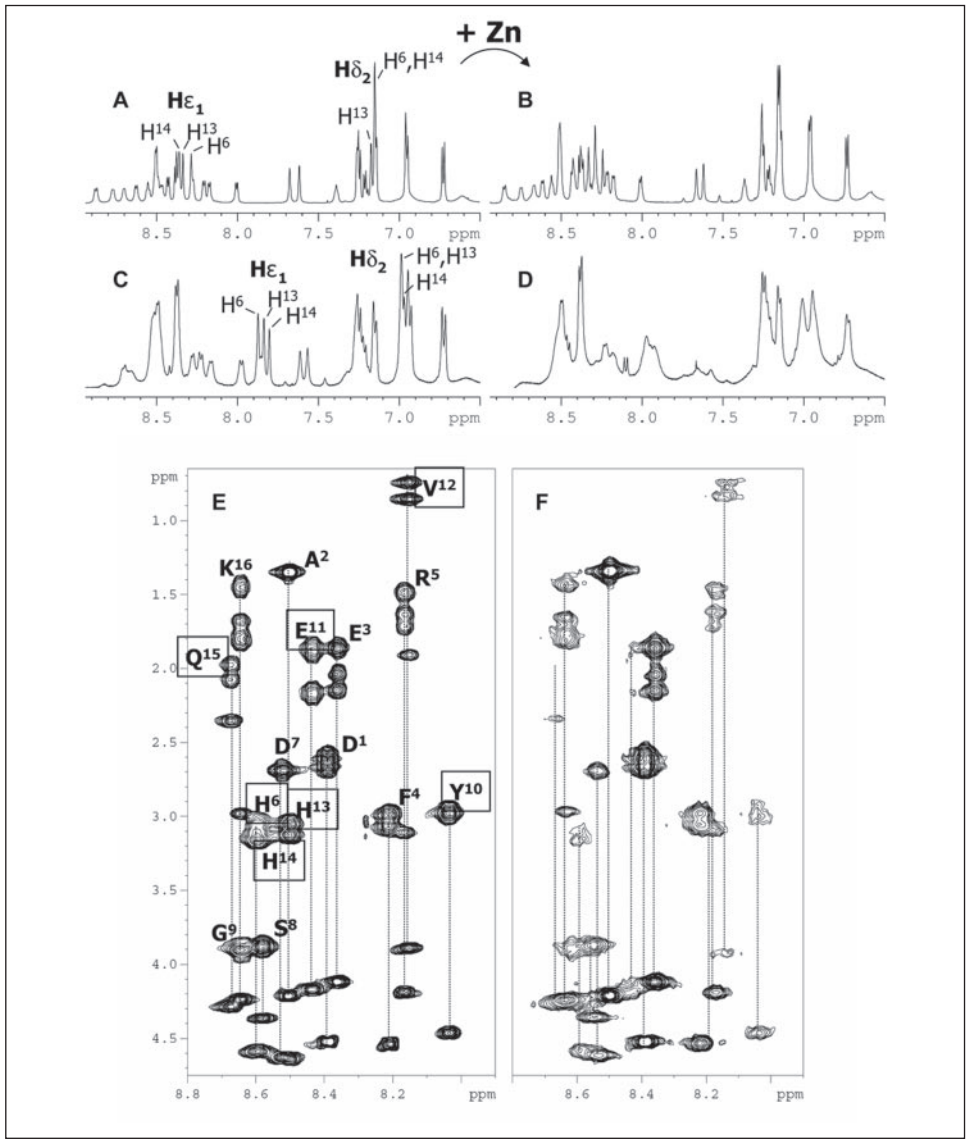

FIGURE 2. **^{1}H NMR spectra of Aβ-(1–16) in the absence and in the presence of Zn^{2+} at pH 6.5 and 7.5.** *A–D,* enlargements of the amide and aromatic proton region of the 400-MHz one-dimensional ^{1}H NMR spectra of 2 mM Aβ-(1–16). *A,* pH 6.5; *B,* pH 6.5, [Zn^{2+}] 3 mM; *C,* pH 7.5; *D,* pH 7.5, [Zn^{2+}] 3 mM. *E* and *F,* two-dimensional TOCSY spectra of 3 mM Aβ-(1–16) at pH 7.5 in the absence (*E*) and in the presence (*F*) of 4.8 mM Zn^{2+}. Amino acid assignments are provided in *E*; *boxes* point those spin systems that undergo the strongest broadening upon Zn^{2+} addition.

before each NMR experiment, and the absence of pH variation over the period of acquisition was checked immediately after. The pK_a values were determined by analyzing the pH titration curves by nonlinear least square fit to the equation $\delta = (\delta_1 + \delta_2 \times 10^{(pH - pK_a)})/(1 + 10^{(pH - pK_a)})$, where δ is the chemical shift of a resonance measured as a function of pH, and δ_1 and δ_2 are its chemical shifts at the lowest and highest pH values, respectively. This procedure was carried out using the software Curve Expert 1.3. The equation used derives from the Henderson-Hasselbalch equation, assuming a rapid equilibrium between protonated and unprotonated forms (50) and considering a noninteracting model (51).

Distance and Dihedral Angle Constraints—Distance constraints resulting from integrated NOESY spectra and φ dihedral angles derived from the $^3J_{HN\text{-}H\alpha}$ coupling constants using the Pardi relation (52) were used for structure calculation. The NOESY experiment with 200 ms of mixing time was selected for distance calculation to get rid of spin diffusion associated with T_1 relaxation. A tolerance range of ±25% of the NMR-derived distances was used to define the upper and lower values of the constraints.

Structure Calculation and Analysis—The three-dimensional structures of Aβ-(1–16) at pH 6.5 in the absence and in the presence of zinc were calculated using simulated annealing and energy minimization protocols in X-PLOR 3.851. Alternatively, the conformational calculations were performed with a general purpose internal coordinate molecular dynamics program ICMD (53) by using the variable target function approach (54) adopted for dynamics in the torsion angle space. The program ICMD was further used to calculate the three-dimensional structure of the Aβ-(1–16)-Zn^{2+} complex. The structures obtained from ICMD calculations are only presented here as final structures.

The molecular dynamics calculations in X-PLOR 3.851 were performed with a target function similar to that used by Nilges *et al.* (55) and a force field adapted for NMR structure determination (parallhdg.pro and topallhdg.pro). When no stereospecific assignments could be made for methyl and methylene protons, the constraints were considered with an appropriate treatment in X-PLOR. Several rounds of structure calculation and assignment were performed to resolve ambiguities. Starting from an extended template structure, a set of 100 structures was calculated. A first phase of 400-ps dynamics (time step = 2 fs) at 1000 K was followed by 80-ps slow cooling step to 100 K (time step = 2 fs; temperature step = 20 K). A weak weight of the van der Waals repulsive term was used at high temperature in order to allow a large conformational sampling. Refinement of the structures was achieved by

using the conjugate gradient Powell algorithm with 7000 cycles of energy minimization, using the CHARMM 22 force field (files topallh22x.pro and parallh22x.pro) (56).

The ICMD program was used with the standard geometry of amino acids and peptide bonds and involved multiple cycles of simulated annealing starting from an arbitrary extended peptide conformation. The AMBER99 all-atom force field parameters (57) were applied, with nonbonded interactions truncated at 6 Å by a force-shift method to maintain reasonable atom-atom distances and avoid any bias from longer range interactions. The Aβ-(1–16) peptide was modeled with all torsion degrees of freedom. According to the variable target function principle (54), all NOE-based distance constraints were first checked for the number of free torsions that separate every particular proton pair. The corresponding number is further referred to as torsion separation. The simulated annealing started from an arbitrary extended conformation obtained by an unrestrained MD simulation under high temperature (7000 K). At the beginning, only constraints of torsion separation one were applied. The following separation levels were added one by one in the course of the protocol when reasonable convergence was achieved for all previous torsion separation levels. As the ICMD protocol does not use pseudoatoms, instead all candidate proton pairs corresponding to a given resonance were analyzed from time to time, and the corresponding constraint was reassigned to the pair with the shortest distance in the current conformation.[4] The structure calculation of the Aβ-(1–16)-Zn^{2+} 1:1 complex was carried out using a strategy including two independent steps. In the first step, the structure of the polypeptide chain only was refined in calculations performed without explicit Zn^{2+} ion and without any assumption on zinc coordination. The second calculation step was used in order to obtain a specific peptide-zinc complex structure with a metal coordination geometry satisfying chemical requirements. The experimental set of constraints used in the first step was updated with additional distance and angle constraints that enforced a tetrahedral ligand coordination of the Zn^{2+} ion. To this end, we added four ambiguous constraints that linked the Zn^{2+} ion with all possible partners. These constraints were arbitrarily assigned the torsion separation one, and they were treated along with other constraints, as explained above. Their geometry was derived from zinc-binding sites of relevant high resolution x-ray structures available in the Protein Data Bank. The following atoms and groups present in the Aβ-(1–16) peptide were considered as potential zinc chelators: N-δ and/or N-ϵ atoms of His^6, His^{13}, and His^{14}, O-δ1–O-δ2 atoms of Asp^1 and Asp^7, and O-ϵ1–O-ϵ2 atoms of Glu^3 and Glu^{11}. These Zn^{2+} ligand hypotheses were in agreement with those authorized by the NMR data obtained. The 2.0 Å harmonic distance constraints were applied for the distance between the Zn^{2+} ion and each of its four chelators. If one of the histidine nitrogens took part in the complex, the Zn^{2+} ion was kept in the plane of the imidazole ring and in the bissector plane of the corresponding nitrogen atom by using additional angle constraints. In this case the other nitrogen of the same imidazole ring was temporarily excluded from the list of possible chelators. In a similar way, an appropriate symmetrical orientation of Zn^{2+} with respect to the Asp and Glu carboxyl groups was ensured. The calculated conformers were analyzed using MOLMOL (58), RASMOL (59), and PROCHECK (60) programs. Their coordinates are deposited in the Protein Data Bank.

Production of Aβ-(1–16) Modified Forms by in Vitro Aging—Aβ-(1–16) (50 μM or 1.50 mM) or $Aβ-(1–16)^{hemi}$ (50 μM) was incubated as described previously (38) in 50 mM Tris-HCl, pH 7.4, containing 0.05% NaN_3 (w/v) either at 37 or 70 °C in the absence or presence of 1 mM EDTA. The *in vitro* aging experiments in the presence of zinc were conducted with the same protocol in the absence of EDTA and in the presence of $ZnCl_2$ with a 1:5 peptide/zinc ratio. Reactions were stopped by freezing the samples at −20 °C. The modified peptide mixtures obtained were analyzed at different incubation times by RP-HPLC on a Shiseido C-18 Capcell Pack, 5 μm, 4.6 × 250-mm column from Interchim (Montluçon, France), using a linear gradient of 10–40% MeOH in 0.1% aqueous trifluoroacetic acid, at a flow-rate of 1 ml/min. Elution was monitored by measuring the absorbance at 226 nm. Molecular masses of the separated species were determined by liquid chromatography-MS using a Discovery®HS C-18, 3 μM, 2.1 × 150-mm analytical column (Supelco, St Quentin-Fallavier, France) coupled to an ESI-hybrid quadrupole time-of-flight mass spectrometer (Q-STAR Pulsar, Applied Biosystems, Courtaboeuf, France). The separation was obtained with a linear gradient of 27–35% MeOH in 0.1% aqueous trifluoroacetic acid over 40 min at a flow rate of 200 μl/min. The same aging protocol was used for the nonacetylated peptide $Aβ-(1–16)^{hemi}$. The modified peptide mixtures resulting from the incubation were analyzed at different incubation times by RP-HPLC, as described above, using a linear gradient of 13–18% ACN in 0.1% aqueous trifluoroacetic acid over 40 min at a flow rate of 1 ml/min.

FIGURE 3. **Main sequential and medium range NOEs observed for Aβ-(1–16) at pH 6.5 in the absence (*black*) and in the presence (*gray*) of Zn^{2+}.** The *thickness* of the *bars* illustrates the relative cross-peak intensities.

Isolation of Aβ-(1–16) Isomers Produced from in Vitro Aging—The modified peptides resulting from incubation of Aβ-(1–16) at 70 °C for 14 days were purified by semi-preparative RP-HPLC on a C-18 Uptisphere, 5 μm, 7.8 × 250-mm column (Interchim, Montluçon, France) with a linear gradient of 27–35% MeOH in 0.1% aqueous trifluoroacetic acid over 40 min at a flow-rate of 2 ml/min. Absorbance was monitored at 226 nm. Purity of the isolated species was checked by RP-HPLC and ESI-MS (Q-STAR Pulsar, Applied Biosystems, Courtaboeuf, France).

Identification of Aβ-(1–16) Isomers Produced from in Vitro Aging—Truncated peptides were identified by ESI-MS in positive mode (Q-STAR Pulsar, Applied Biosystems, Courtaboeuf, France). The peptide sequences were checked by collision-induced dissociation experiments. Isoaspartic acid residues within Aβ-(1–16) isomers were quantified by enzymatic methylation catalyzed by the L-isoaspartyl methyltransferase, using the Isoquant® protein deamidation kit (Promega, Charbonnieres, France), as described previously (61). Briefly, 10 μl of a 7.5 μM peptide solution in water were added to the reaction buffer (NaH_2PO_4/Na_2HPO_4 125 mM, pH 6.8, 1.25 mM EGTA, 0.005% NaN_3, 0.2% Triton X-100) containing L-isoaspartyl methyltransferase and 0.1 mM *S*-adenosyl-L-methionine. Enzymatic reactions were performed in duplicate at 30 °C for 30 min and stopped by adding 10 μl of 0.3 M phosphoric acid. Solutions were centrifuged at 10,000 × *g* for 8

[4] T. Malliavin *et al.*, manuscript in preparation.

TABLE 1

Structural statistics of the refined NMR structures of Aβ-(1–16) in different environments

Each presented NMR structure was calculated using the ICMD program and corresponds to the group of 20 refined conformers.

Environments	PB[a]	PB-Zn[b]	
		Protocol 1[c]	Protocol 2[c]
Target function (Å²)	1.60 ± 0.36	3.10 ± 0.80	3.30 ± 0.40
Zinc tetrahedral coordination constraints			
Total			17
Upper distance constraints			4
Planar angle constraints			13
NMR upper distance constraints			
Nonambiguous			
Total	179	253	253
Intra-residue	117	145	145
Sequential	50	75	75
Medium range ($i - j < 5$)	12	29	29
Constraints per residue	11.2	15.8	15.8
Ambiguous			
Total	22	29	29
Constraints per residue	1.4	1.8	1.8
ϕ-torsion angle constraints	5	6	6
Maximum violations			
ϕ-torsion angle constraints (°)	0	0	4.4 ± 1.1
Upper distance constraints (Å)	0.60 ± 0.15	0.67 ± 0.10	0.67 ± 0.05
No. constraint violations >0.3 Å	7 ± 3	7 ± 3	7 ± 3
No. constraint violations >0.2 Å	14 ± 3	17 ± 3	17 ± 3
Ramachandran plot analysis			
Residues in most favored regions (%)	85 ± 8	85 ± 8	75 ± 5
Residues in additionally allowed regions (%)	15 ± 8	15 ± 8	25 ± 5
Structural precision (all residues)			
All atom r.m.s.d.[d] (Å)	4.17	2.46	1.87
Backbone atom[b] r.m.s.d. (Å)	3.08	1.39	0.92
Structural precision (residues 4–15)			
All atom r.m.s.d. (Å)	3.28	1.65	1.14
Backbone N, C-α, C′ atom r.m.s.d. (Å)	1.84	0.72	0.27
Structural precision (residues 4–8)			
All atom r.m.s.d. (Å)	2.71	1.40	1.30
Backbone atom[c] r.m.s.d. (Å)	1.19	0.39	0.22
Structural precision (residues 9–15)			
All atom r.m.s.d. (Å)	1.00	1.14	0.70
Backbone atom[c] r.m.s.d. (Å)	0.29	0.36	0.14

[a] PB indicates phosphate buffer, pH 6.5.
[b] PB-Zn indicates phosphate buffer, pH 6.5, in the presence of Zn^{2+} with a 1:1.5 Aβ(1–16)/Zn^{2+} ratio.
[c] Protocol 1 indicates calculations without any constraints related to zinc binding; protocol 2 indicates calculations using in addition the distance and planar angle constraints described under "Materials and Methods" intended to enforce the tetrahedral coordination of one zinc cation in the Aβ-(1–16)-Zn^{2+} complex.
[d] r.m.s.d. indicates root mean square deviation.

min at 4 °C. Supernatants were kept at 4 °C until RP-HPLC analyses, which were performed within the day using a C-18 Uptisphere, 5 μm, 4.6 × 250-mm column (Interchim, Montluçon, France) eluted with a linear gradient of 10–30% MeOH in NaH_2PO_4/Na_2HPO_4 10 mM, pH 6.2, over 20 min at a flow-rate of 1 ml/min. Absorbance was monitored at 260 nm. Iso-Asp residues within the incubation products were quantified by plotting the *S*-adenosylhomocysteine peak intensity on a standard curve drawn up from RP-HPLC profiles of different *S*-adenosylhomocysteine dilutions.

Before N-terminal sequencing, partial hydrolysis of the Aβ-(1–16) isomers was performed in trifluoroacetic acid at 48 °C (62). The peptides cleaved between residues 1 and 2 were purified by RP-HPLC (Uptisphere, Interchim, 5 μm, 4.6 × 250 mm) with a linear gradient of 10–25% ACN in 0.1% aqueous trifluoroacetic acid over 15 min, at a flow rate of 1 ml/min. They were then resuspended in MilliQ™ water (Millipore, Saint-Quentin-en-Yvelines, France), and each sample was loaded and argon-dried on a Biobrene-coated filter before being subjected to Edman degradation on a Procise 492 automatic protein sequencer (PerkinElmer Life Sciences).

Absolute configuration of the amino acids of the Aβ-(1–16) isomers was determined by gas chromatography (GC) analysis of the *N*-trifluoroacetylisopropyl ester derivatives of the amino acids present in the total hydrolysates, as described previously (63). GC analyses were performed with a 5890 series II chromatograph (Hewlett-Packard, Les Ulis, France) equipped with a flame ionization detector, on a 25-m length, 0.2-mm internal diameter, 0.12-μm film thickness Chirasil-L-Val (*N*-propionyl-L-valine *tert*-butylamide polysiloxane) quartz capillary column (Varian, Les Ulis, France), using helium as carrier gas at a flow rate of 1.25 ml/min. Injector and detector temperatures were maintained at 300 °C, and the oven temperature was programmed from 50 to 310 °C at a rate of 3 °C/min and then kept at 310 °C for 8 min. The L- or D-configuration of the amino acids was determined by comparing the GC profiles obtained with those of standard L- or D-amino acids derivatized in the same conditions.

RESULTS

Structures of Aβ-(1–16) and Aβ-(1–16)-Zn^{2+} in Aqueous Solution—One-dimensional ^1H NMR spectra of Aβ-(1–16) were recorded over the 0.3–4 mM range of concentrations either in sodium phosphate or Tris-d_{11}/HCl buffers at pH 7.4 and 6.5. No differences in line widths or chemical shifts could be detected, supporting the absence of aggrega-

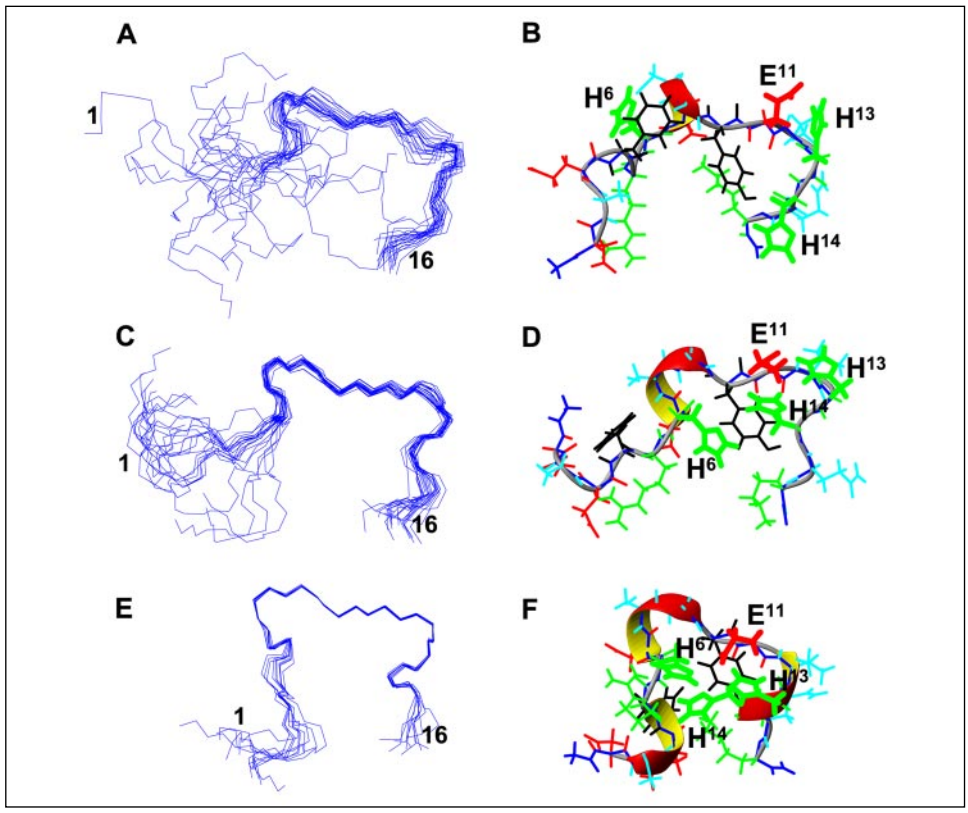

FIGURE 4. Three-dimensional ICMD structure of Aβ-(1–16) at pH 6.5 in the absence (*A* and *B*) and in the presence (*C–F*) of Zn^{2+}. The structures in *C* and *D* result from calculations performed without any constraints related to the zinc cation, whereas *E* and *F* were obtained after introduction of additional constraints relative to the zinc ion coordination. *A, C,* and *E,* overlays of the backbone atoms for the 20 selected structures (residues 6–15); *B, D,* and *F,* typical structures showing the side chain orientation (backbone in *blue*, basic residues in *green*, acidic residues in *red*, aromatic residues in *black*, and other residues in *cyan*). The side chains of His^6, Glu^{11}, His^{13}, or His^{14} are shown with broader bond lines.

tion of the peptide at such concentrations in agreement with our previous CD data (34).

Spin system identification and complete NMR ^1H assignments (supplemental Table A) were generally obtained from DQF-COSY, TOCSY, and NOESY experiments, using the sequential assignment protocol (64). Spectra recorded at 278 K were primarily used for assignments, and spectra measured at other temperatures, as well as HSQC and HMBC data, were used to resolve ambiguities (see ^{13}C assignments in supplemental Table B).

The conformational parameters were analyzed for Aβ-(1–16) at pH 7.4. They were not indicative of any regular secondary structure elements in the peptide conformation (Fig. 1). However, the dNN($i,i+1$) and dα N($i,i+2$) NOEs displayed in the regions 2–5 and 7–13, and in particular the intense dNN between Gly^9–Tyr^{10}, Tyr^{10}–Glu^{11}, and Glu^{11}–Val^{12} (data not shown), suggested that these regions folded into a noncanonical structure.

The preliminary analysis of Aβ-(1–16) by CD showed that it formed a soluble and stable complex with Zn^{2+} ions in the pH 6.0–8.0 range, leading to a conformational change, whereas the homologous peptide with unprotected N and C termini precipitated upon zinc addition (34). Therefore, Aβ-(1–16) was chosen for a complete NMR analysis in the absence and in the presence of Zn^{2+}, in order to characterize the structural change of the N-terminal region 1–16 of Aβ upon zinc binding. The NMR conformational parameters were acquired at 278 K to ensure observation of the amide protons of His^6 and His^{14}, which were not observable at higher temperatures, due to amide proton exchange in the considered pH range. Given the potential contribution of the three histidines to the zinc coordination sphere, their pK_a values were first measured in order to determine whether these residues were in ionized or neutral form under physiological pH values. The pK_a values were calculated from nonlinear least square fit of H-δ2 and H-ϵ1 proton titration curves to the Henderson-Hasselbalch equation, and the values 7.0, 6.9 and 6.8 ± 0.1 were assigned to His^6, His^{13}, and His^{14}, respectively. An equilibrium between protonated and deprotonated imidazole rings was observed in the 6.0–8.0 pH range (supplemental Fig. S1) that corresponded to the pH domain where the zinc-induced conformational change and the soluble Aβ-(1–16)-Zn^{2+} complex had been previously characterized by CD (34). Addition of Zn^{2+} to a 2 mM Aβ-(1–16) sample, either in phosphate buffer at pH >6 or in Tris-d_{11}/HCl buffer at pH 5.8 led to the formation of a low amount of precipitate. From our previous analysis of the complex by CD and ESI-MS, this precipitate could be identified as the insoluble fraction of the Aβ-(1–16)-Zn^{2+} 1:1 complex formed at the higher concentration used for NMR. The supernatant was thus submitted to the NMR experiments. One-dimensional ^1H NMR recordings over the 0.3–3.5 mM range of concentrations discarded the presence of a change in the aggregation state and was in favor of a monomeric state of the 1:1 complex at the 2 mM peptide concentration used for the structure analysis. The ^1H one-dimensional NMR spectra of Aβ-(1–16) recorded either in the absence or in the presence of 1.5 Zn^{2+} equivalents in sodium phosphate buffer at pH 6.5 and 7.5 did not illustrate any significant Zn^{2+}-induced change in the chemical shifts (Fig. 2, *A--D*). However, a strong and selective peak broadening was observed at pH 7.5 (Fig. 2, *D* and *F*). This mainly concerned region 5–15, whereas the N-terminal region 1–4 remained unaffected. The three histidines were particularly affected, with a complete disappearance of the signals involving the amide protons and H-δ2 and H-ϵ1. In addition, the spin systems of Tyr^{10}, Glu^{11}, and Val^{12} nearly disappeared.

Such a peak broadening, similar to that already observed by Curtain *et al.* (28) upon adding Zn^{2+} to a solution of Aβ-(1–28) could be indicative of exchange between zinc-complexed and uncomplexed Aβ-(1–16). The absence of any change in the rest of the spectrum was in agreement with the monomeric state of the complex analyzed and indicated that the presence of soluble oligomers that could have resulted in broadened resonances was negligible. Finally, pH 6.5, which allowed good quality

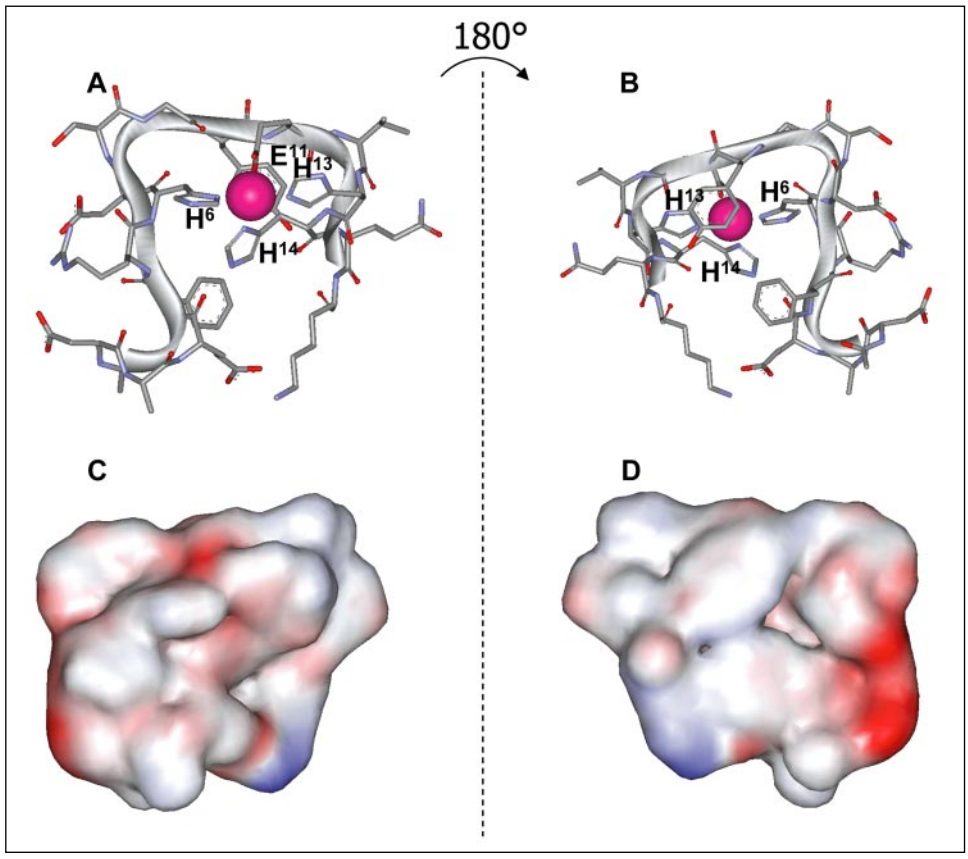

FIGURE 5. **Structure of the Aβ-(1–16)-Zn^{2+} complex at pH 6.5 calculated with the ICMD protocol.** *A* and *B*, views showing the location of the zinc ion, which is coordinated through the imidazole nitrogens of the three histidine, His^6, His^{13}, and His^{14}, side chains and the carboxylate of the Glu^{11} side chain. *C* and *D*, corresponding electrostatic molecular surface of the complex; *C*, view is rotated 180° about the *x* axis relative to the *A* view. *Blue* and *red* correspond to negatively and positively charged areas, respectively.

spectra and was still included in the protonation/deprotonation pH range of the three histidines (supplemental Fig. S1), was selected for investigation of the three-dimensional structure of the apoAβ-(1–16) and the Aβ-(1–16)-Zn^{2+} complex. Although most of the conformational parameters of Aβ-(1–16), *i.e.* H-α- and C-α-CSD, $^3J_{HN\text{-}H\alpha}$ and $\Delta\delta/\Delta T_{HN}$, were unchanged upon Zn^{2+} addition, a number of additional specific NOEs were observed in the presence of Zn^{2+} (Fig. 3), which suggested a structural change.

The three-dimensional structures of the apoAβ-(1–16) and the Aβ-(1–16)-Zn^{2+} complex were calculated by NMR-restrained molecular modeling, using the constraints summarized in Table 1. The apoAβ-(1–16) appeared poorly structured in the N-terminal 1–6 region (Fig. 4*A*), whereas an irregular structure was characterized in the 7–15 part, including a turn centered at residues 7–8. The 20 selected structures displayed a good fit of the side chains in the C-terminal region. Their orientation suggested the presence of stabilizing intramolecular hydrogen bonds involving the pairs Asp^7/Lys^{16} and Glu^{11}/His^{13}, as well as the backbone carbonyl group of His^{14} and the Tyr^{10} side chain (Fig. 4*B*). In the presence of Zn^{2+}, the modeling of the Aβ-(1–16) structure using X-PLOR or ICMD programs without introducing any constraints related to the cation binding resulted in a more compact structure (Fig. 4*C*). Compared with the apoAβ-(1–16) folding, the structure of the N-terminal region was better defined, and a global reorientation of most side chains toward the inside of the structure was observed, which particularly concerned those of all three histidines (Fig. 4*D*). The ICMD protocol (53) was used to assign the peptide/Zn^{2+}-binding sites and obtain the three-dimensional structure of the Aβ-(1–16)-Zn^{2+} complex (Fig. 4, *E* and *F*, and Fig. 5). In most of the selected structures, the Asp^7–Gly^9 region adopted an irregular 3_{10} helical structure (Fig. 4*F*). The Zn(II) cation was tetrahedrally coordinated to His^6, His^{13}, and His^{14} through their N-δ1, N-ϵ2, and N-δ1 atoms, respectively, and to Glu^{11} through its carboxylate. It is worth noting the coordination sphere proposed from our calculation conveniently fits the ^{111}Cd NMR data obtained by Mekmouche *et al.* (36). In all the selected structures, the Phe^4 residue appeared to be located in the inner core of the structure, and Tyr^{10} was systematically located on the face opposed to the zinc atom. The binding sites thus obtained corresponded to the more broadened spin systems displayed on the TOCSY spectrum registered in the presence of Zn^{2+} (Fig. 2, *D* and *F*). An analysis of the surface features of the complex (Fig. 5, *C* and *D*) showed that most of the surface is hydrophobic or neutral, with a negatively charged patch located near the N terminus (Asp^1 and Glu^3) and a single restricted positively charged region due to Lys^{16}. This is in agreement with the fact that all positively charged residues present in Aβ-(1–16) reoriented toward the inner core of the complex.

In Vitro Aging of Aβ-(1–16) in the Absence and in the Presence of Zn^{2+} Ions and Subsequent Isomerizations and Racemizations—In vitro aging of Aβ-(1–16) was performed by incubation at pH 7.4 and 37 °C, either in the absence or in the presence of Zn^{2+}. In order to accelerate the rate of succinimide formation (38) and to facilitate the identification of a maximal range of modified species, another set of experiments was conducted at 70 °C. The aging experiments at 37 °C were conducted over an incubation period of 70 and 130 days in the absence and in the presence of Zn^{2+}, respectively (Fig. 6, *A* and *B*), whereas this incubation period could be shortened to 14 days at 70 °C. The chromatograms obtained in the absence and in the presence of EDTA were similar (data not shown), ruling out the contribution to the chemical modifications observed of trace metal contaminants, such as copper-induced redox processes.

The Asp^1- and Asp^7-isomerized and/or racemized species formed at 70 °C (Fig. 6*C*) were identified from a panel of experiments, including (i) L-isoaspartyl methyltransferase-assisted quantification of isoaspartate residues, (ii) Edman sequencing, and (iii) GC analysis on a chiral capil-

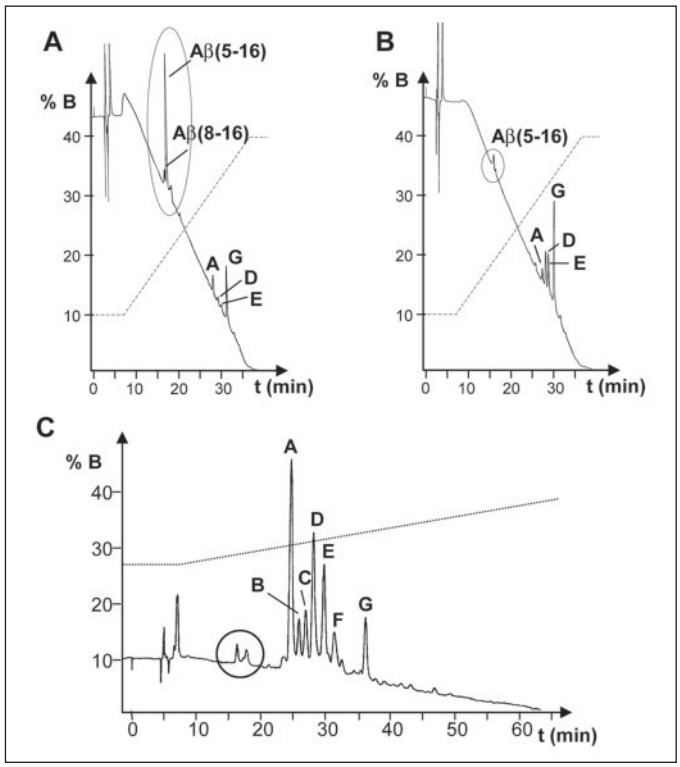

FIGURE 6. **RP-HPLC profiles of Aβ-(1–16) obtained upon *in vitro* aging.** *A* and *B,* analytical chromatograms obtained after 42 days of incubation at pH 7.4, 37 °C, in the absence of Zn^{2+} (*A*) and after 128 days incubation in the presence of Zn^{2+} (*B*). *C,* semi-preparative chromatogram recorded after 14 days incubation at pH 7.4 and 70 °C. The *circled* species correspond to truncated forms of Aβ-(1–16). *Peaks A–F* correspond to the isomers of Aβ-(1–16) (see Table 2), with *peak G* being unmodified Aβ-(1–16). The MeOH percentages in the gradients used for separations are represented as *dotted lines*.

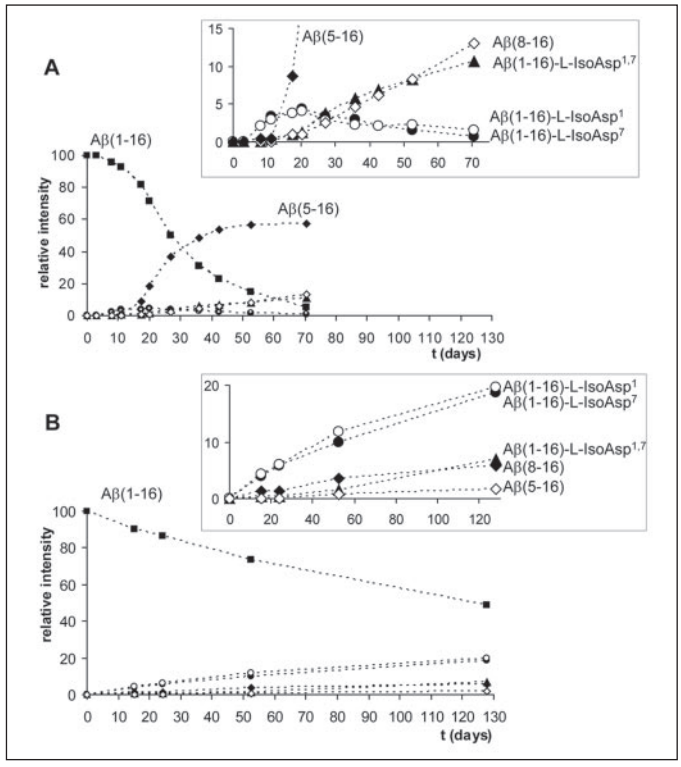

FIGURE 7. **Relative intensities of the major species formed upon *in vitro* aging in the absence (*A*) and in the presence (*B*) of Zn^{2+} and detected by RP-HPLC as a function of incubation time.** Captions show enlargements of the evolution of the minor species as a function of incubation time.

lary column of the derivatized amino acids obtained in the total acid hydrolysate (Table 2). The A, D, and E species, which are the three major isomers produced, were assigned to Aβ-(1–16)-L-iso-Asp^{1,7}, Aβ-(1–16)-L-Iso-Asp^{7}, and Aβ-(1–16)-L-iso-Asp^{1}, respectively. Furthermore, liquid chromatography-MS analysis revealed the presence of N- or C-truncated peptides (Fig. 6*C, circled peak*), which were identified from both their *m/z* ratios and MS/MS data as Aβ-(2–16), Aβ-(1–7), and Aβ-(1–6) (data not shown).

In vitro aging of the nonacetylated Aβ-(1–16)^{hemi} peptide also led to the formation of truncated and isomerized species at 70 °C, but peak overlapping in the HPLC profiles rendered the attribution incomplete (data not shown). The Aβ-(2–16)-, Aβ-(1–7)-, and Aβ-(1–6)-truncated peptides were detected, as for Aβ-(1–16) aging, but the major truncated species formed was Aβ-(3–16). Successful Edman sequencing of this last peptide indicated the absence of the N-terminal pyroglutamate residue in this truncated form.

At 37 °C, the truncated peptides appeared favored as compared with the isomerized species, Aβ(5–16) being the major modified species from 20 days of incubation (Fig. 6*A* and 7*A*). In addition, the racemizations of L-Asp or L-iso-Asp residues to their D-isomers were totally absent. The presence of Zn^{2+} ions in the incubation medium significantly altered the kinetic profile of the *in vitro* aging at 37 °C by disfavoring truncations at the advantage of isoaspartate formation at positions 1 and 7 in the sequence (Fig. 6*B* and Fig. 7*B*). By contrast, the presence of Zn^{2+} ions in the incubation medium was without effect on the nature and the relative abundances of the species formed from Aβ-(1–16) at 70 °C (data not shown).

The conformational parameters of Aβ-(1–16)-L-iso-Asp^{7}, one of the major species formed in the presence of Zn^{2+}, were quite similar to those of Aβ-(1–16) (Fig. 1). Local changes in the His^{6}–Ser^{8} region were observed because of the presence of L-iso-Asp^{7}, as illustrated by the CSD profiles (Fig. 1, *B* and *C*). Furthermore, as already observed for L-iso-Asp-containing proteins (65), this residue triggered a change in the intensity of sequential NOEs between residues 7 and 8, with a strengthened dβ N connectivity and a weakened dα N connectivity (data not shown). However, the observed changes in the NMR parameters appeared to be local and not to express a perturbation of the global peptide fold. One-dimensional ^{1}H and TOCSY spectra of Aβ-(1–16)-L-iso-Asp^{7} were performed in the presence of Zn^{2+} ions in order to assess the effect of isoaspartate on the Aβ-(1–16)-Zn^{2+} interaction. Because a precipitate formed at pH values above 6, the spectra were recorded at pH 5.8. They showed a particularly strong broadening of the L-iso-Asp^{7} signals, which almost disappeared from the spectra; His^{6} and residues 10–14 were also affected (data not shown). These results indicated that the modified L-iso-Asp^{7} residue did not prevent the interaction and even was contributing to the zinc coordination.

DISCUSSION

The N-terminal 1–16 part of Aβ is a flexible region that remains accessible in amyloid deposits (14, 15) and is involved in the zinc binding capacity and protein aging propensity of Aβ. In this study, we characterized for the first time the three-dimensional structure of the soluble Aβ-(1–16)-Zn^{2+} complex as well as the chemical modifications of this region of Aβ upon protein aging.

Structuration of Aβ-(1–16) Upon Zinc Binding—In phosphate buffer at pH 6.5, the apoAβ-(1–16) shows a rather well defined structure, particularly in region 7–15, but without any canonical element. The addition of Zn^{2+} to the solution mainly affects the Tyr^{10}–Gln^{15} region and particularly the H-δ2 and H-ε1 resonances of all three histidines, in agreement with previous data on Aβ-(1–28) (28). The Aβ-(1–16) struc-

TABLE 2

Identification of the isomers of Aβ-(1–16) produced upon *in vitro* aging at pH 7.4 and 70 °C

The outcome of the L-isoaspartyl methyltransferase (PIMT)-catalyzed methylation, Edman sequencing, and chiral GC results is shown. The asterisk indicates a yield decrease in Edman sequencing.

Isomer	No. (L)-iso-Asp (PIMT)	Sequence Edman	Asp/iso-Asp configuration (GC)	Residues identified	
				Position 1	Position 7
A	2	AEFRH	2 (L)	(L)-iso-Asp	(L)-iso-Asp
B	1	AEFRH	1 (L), 1 (D)	(D)-Asp or (D)-iso-Asp	(L)-iso-Asp
C	1	AEFRH	1 (L), 1 (D)	(D)-Asp or (D)-iso-Asp	(L)-iso-Asp
D	1	AEFRH	2 (L)	(L)-Asp	(L)-iso-Asp
E	1	AEFRHDSGYE…	2 (L)	(L)-iso-Asp	(L)-Asp
F	0	AEFRHD*SGYE…	1 (L), 1 (D)	(L)-Asp	(D)-Asp
G	0	AEFRHDSGYE…	2 (L)	(L)-Asp	(L)-Asp

ture becomes more compact upon zinc binding. The three-dimensional structure of the Aβ-(1–16)-Zn^{2+} soluble 1:1 complex calculated from the NMR constraints reveals His^6, Glu^{11}, His^{13}, and His^{14} as the four ligands involved in the zinc coordination sphere. Such a motif of zinc attachment is reminiscent of a motif identified previously in the case of short peptides designed to bind zinc ions (66). The identification of the three histidines as the zinc ligands does not contradict previous studies using various spectroscopic techniques, which proposed that one to all three histidines in this region of Aβ acted as metal-binding sites (31–33, 36). The identification of the fourth zinc chelator is much more debated. The present calculation of the complex identifies Glu^{11} as the fourth partner, acting through its carboxylate side chain. In our previous MS study on the Aβ-(1–16)-Zn^{2+} complex (35), Arg^5 was proposed as the additional ligand. This discrepancy with the present work is most likely attributable to the different acidic/basic properties of the amino acids in the gas phase and in solution (67). Tyr^{10} has been also suggested previously as a possible ligand participating in Cu^{2+} or Zn^{2+} chelation by Aβ (28, 32). In the structure obtained here for the Aβ-(1–16)-Zn^{2+} soluble 1:1 complex, Tyr^{10} is excluded from the coordination sphere and is located on the opposite face from the Zn^{2+} ion. This is in agreement with Mekmouche *et al.* (36), who also excluded the involvement of Tyr^{10} in the coordination sphere from both NMR and absorption spectroscopy data. In this last study, Asp^1 was proposed as the fourth coordination site of the zinc ion in Aβ-(1–16) at pH 8.7 (36). This is not consistent with our NMR data at pH 6.5 and 7.5. Those exclude Asp^1 as metal chelator, because (i) the corresponding NMR signals were not broadened upon zinc addition, and (ii) this residue was not selected as contributing to the zinc coordination sphere in our structure calculations, although it was considered as a potential ligand. The lower pH and the N-terminal acetylation of Aβ-(1–16) in our study can contribute to understanding this difference.

From our results, region 9–15, which contains three of the zinc ligands Glu^{11}, His^{13}, His^{14}, appears as a prefolded region in Aβ-(1–16). The fourth ligand in the zinc coordination sphere, His^6, is provided by region 4–8 of Aβ-(1–16), which is poorly structured. The N-terminal zinc binding region of Aβ thus behaves as an independent folding unit. Zinc binding to apoAβ-(1–16) appears to stabilize the preformed structure of region 9–15 and to induce the folding of the N-terminal region into an irregular 3_{10} helix. The irregular helical structure displayed by most of the structures calculated here for Aβ-(1–16) suggests that zinc binding to Aβ promotes its helical rather than β-sheet conformation, as also proposed for longer Aβ peptides (28, 68). In light of our results, the conformational change of Aβ-(1–16) in the presence of zinc appears to be rather a stabilization and structuration of a poorly preformed structure than a drastic transconformation. This trend is in agreement with Curtain *et al.* (28) and with our previous observation that a structure stabilization of Aβ-(1–16) upon Zn^{2+} binding induces a better recognition of this region of Aβ by monoclonal antibodies (47).

In the absence of zinc, Aβ-(1–16) displays a bend in its central region, as illustrated by the intense dNN($i,i+1$) NOEs between Gly^9 and Val^{12}. This bending has also been described for the full-length Aβ and has been proposed to contribute to Aβ fibrillation by promoting the formation of salt bridges involving the histidine and aspartic/glutamic acid side chains (69). From our study, zinc binding appears to stabilize this bended structure, which could reinforce the hypothesis of the involvement of zinc in Aβ aggregation (19–21, 36). However, the nonfibrillar nature of Aβ aggregates formed upon zinc addition (26, 27) contradicts this interpretation. Furthermore, the involvement of the histidines in zinc binding would rather compete with the formation of salt bridges with aspartic/glutamic acid side chains. Therefore, we propose that zinc binding would not be implicated in Aβ fibrillogenesis but would rather occur after amyloid deposition as a result of the accessibility of the Aβ N-terminal region within fibrils. In this context, zinc binding-induced aggregation of Aβ would result from another mechanism, such as the formation of intermolecular histidine-metal-histidine bridges (18, 28).

Our CD (34) and NMR data have shown that Aβ-(1–16) is monomeric in the 5 μM to 1 mM concentration range. The absence of oligomerization upon zinc binding has been shown previously by size exclusion chromatography (36). This trend is also emphasized by the absence of variation in Aβ-(1–16) NMR chemical shifts and of unspecific NMR signal broadening upon zinc addition. Similarly, Curtain *et al.* (28) have characterized 1:1 monomeric complexes with copper for Aβ-(1–28) and Aβ-(1–40). In the conditions of our study, zinc binding to Aβ-(1–16) appears to lead to the soluble monomeric complex accompanied by a small amount of insoluble aggregates, as proposed by Miura *et al.* (32).

Protein Aging-induced Modifications of Aβ-(1–16)—Because age-related peptide modifications are suggested to participate in the AD pathogenesis, *in vitro* aging of Aβ-(1–16) has been investigated here. Numerous modifications of the synthetic peptide are observed, *i.e.* truncations, isomerizations, and racemizations. Truncated peptides, including an N-terminal pyroglutamate at positions 3 and 11 of Aβ, are species that have been detected within amyloid fibrils (71). Such species are not formed here during the *in vitro* aging process of Aβ-(1–16) or $Aβ\text{-}(1–16)^{hemi}$ at 37 °C. Thus, the truncated molecular forms detected within fibrils presumably represent by-products of metabolic intermediates toward degradation and are not produced spontaneously upon protein aging.

The incorporation of iso-Asp residues is suggested to increase the tendency to form β-sheet in amyloid peptides (41, 70). Here we observe that the isomerization of L-Asp^7 to L-iso-Asp leads to a local conformational change in the region His^6–Ser^8 but does not affect the overall structure of the peptide. More interestingly, the presence of Zn^{2+} ions significantly changes the chemical modification profile of Aβ-(1–16) upon the *in vitro* aging process at 37 °C, by favoring isomerizations at the expense of truncations. This trend suggests that the association of

the modified peptides Aβ-(1–16)-L-iso-Asp[1], Aβ-(1–16)-L-iso-Asp[7], and Aβ-(1–16)-L-iso-Asp[1,7] with Zn^{2+} ions displaces the equilibrium of the Aβ-(1–16) isomerization reactions toward the formation of L-iso-Asp species. Furthermore, Aβ-(1–16)-L-iso-Asp[7], one of the two major modified species generated upon protein aging, appears to bind Zn^{2+} with a different coordination mode, involving the L-iso-Asp[7] residue itself. Finally, the presence of a peptide bond before Asp[1] does not affect the propensity of this residue to undergo isomerizations/racemizations, because the nonacetylated Aβ-(1–16)[hemi] also exhibits aging-related modifications at Asp[1] and Asp[7].

The impact of the aging-related modifications of the aspartate residues on both the conformation of Aβ-(1–16) and its zinc binding capacity has been subsequently assessed here. Altogether, our results reflect the high potential of chemical and conformational modifications of region 1–16 of Aβ upon both aging and zinc binding, which could partly account for its important structural heterogeneity within amyloid fibrils.

Implications for Therapeutic Approaches with Region 1–16 of Aβ as Target—The occurrence of truncated, isomerized, and racemized species of Aβ and of zinc-bound species within amyloid deposits must be considered in the frame of a therapeutic approach targeting the N-terminal region of Aβ. On the one hand, the modified species of Aβ could be used as immunological targets, while avoiding autoimmune response because of the recognition of the soluble Aβ. The established potentiality to target specifically a particular isomer of Aβ present within amyloid deposits (43) suggests the applicability of such an approach to isomerized species of Aβ. On the other hand, the high zinc content within amyloid plaques might not be adverse but even favorable to the interaction of Aβ with anti-Aβ antibodies, which constitutes a positive trend in the frame of an epitope-based vaccination approach (16, 47).

Acknowledgments—We thank Prof. D. Davoust (IRCOF, Rouen, France) for access to the NMR facility. We are grateful to Prof. A. Ménez (DIEP, CEA, Saclay, France) for access to the automatic protein sequencer and for helpful discussions. We also thank Dr R. Thaï for careful technical assistance in Edman sequencing.

REFERENCES

1. Barrow, C. J., and Zagorski, M. G. (1991) *Science* **253,** 179–182
2. Zagorski, M. G., and Barrow, C. J. (1992) *Biochemistry* **31,** 5621–5631
3. Talafous, J., Marcinowski, K. J., Klopman, G., and Zagorski, M. G. (1994) *Biochemistry* **33,** 7788–7796
4. Lee, J. P., Stimson, E. R., Ghilardi, J. R., Mantyh, P. W., Lu, Y. A., Felix, A. M., Llanos, W., Behbin, A., Cummings, M., Van Criekinge, M., Timms, W., and Maggio, J. E. (1995) *Biochemistry* **34,** 5191–5200
5. Marcinowski, K. J., Shao, H., Clancy, E. L., and Zagorski, M. G. (1998) *J. Am. Chem. Soc.* **120,** 11082–11091
6. Sticht, H., Bayer, P., Willbold, D., Dames, S., Hilbich, C., Beyreuther, K., Frank, R. W., and Rosch, P. (1995) *Eur. J. Biochem.* **233,** 293–298
7. Coles, M., Bicknell, W., Watson, A. A., Fairlie, D. P., and Craik, D. J. (1998) *Biochemistry* **37,** 11064–11077
8. Shao, H., Jao, S., Ma, K., and Zagorski, M. G. (1999) *J. Mol. Biol.* **285,** 755–773
9. Zhang, S., Iwata, K., Lachenmann, M. J., Peng, J. W., Li, S., Stimson, E. R., Lu, Y., Felix, A. M., Maggio, J. E., and Lee, J. P. (2000) *J. Struct. Biol.* **130,** 130–141
10. Choo, L. P., Wetzel, D. L., Halliday, W. C., Jackson, M., LeVine, S. M., and Mantsch, H. H. (1996) *Biophys. J.* **71,** 1672–1679
11. Malinchik, S. B., Inouye, H., Szumowski, K. E., and Kirschner, D. A. (1998) *Biophys. J.* **74,** 537–545
12. Serpell, L. C., Fraser, P. E., and Sunde, M. (1999) *Methods Enzymol.* **309,** 526–536
13. Ellis, R. J., and Pinheiro, T. J. (2002) *Nature* **416,** 483–484
14. Petkova, A. T., Ishii, Y., Balbach, J. J., Antzutkin, O. N., Leapman, R. D., Delaglio, F., and Tycko, R. (2002) *Proc. Natl. Acad. Sci. U. S. A.* **99,** 16742–16747
15. Kheterpal, I., Williams, A., Murphy, C., Bledsoe, B., and Wetzel, R. (2001) *Biochemistry* **40,** 11757–11767
16. McLaurin, J., Cecal, R., Kierstead, M. E., Tian, X., Phinney, A. L., Manea, M., French, J. E., Lambermon, M. H., Darabie, A. A., Brown, M. E., Janus, C., Chishti, M. A., Horne, P., Westaway, D., Fraser, P. E., Mount, H. T., Przybylski, M., and St George-Hyslop, P. (2002) *Nat. Med.* **8,** 1263–1269
17. Frenkel, D., Balass, M., and Solomon, B. (1998) *J. Neuroimmunol.* **88,** 85–90
18. Bush, A. I. (2003) *Trends Neurosci.* **26,** 207–214
19. Mantyh, P. W., Ghilardi, J. R., Rogers, S., DeMaster, E., Allen, C. J., Stimson, E. R., and Maggio, J. E. (1993) *J. Neurochem.* **61,** 1171–1174
20. Bush, A. I., Pettingell, W. H., Multhaup, G., de Paradis, M., Vonsattel, J. P., Gusella, J. F., Beyreuther, K., Masters, C. L., and Tanzi, R. E. (1994) *Science* **265,** 1464–1467
21. Esler, W. P., Stimson, E. R., Jennings, J. M., Ghilardi, J. R., Mantyh, P. W., and Maggio, J. E. (1996) *J. Neurochem.* **66,** 723–732
22. Lovell, M. A., Robertson, J. D., Teesdale, W. J., Campbell, J. L., and Markesbery, W. R. (1998) *J. Neurol. Sci.* **158,** 47–52
23. Suh, S. W., Jensen, K. B., Jensen, M. S., Silva, D. S., Kesslak, P. J., Danscher, G., and Frederickson, C. J. (2000) *Brain Res.* **852,** 274–278
24. Cuajungco, M. P., and Faget, K. Y. (2003) *Brain Res. Brain Res. Rev.* **41,** 44–56
25. Cuajungco, M. P., Frederickson, C. J., and Bush, A. I. (2005) *Subcell. Biochem.* **38,** 235–254
26. Yoshiike, Y., Tanemura, K., Murayama, O., Akagi, T., Murayama, M., Sato, S., Sun, X., Tanaka, N., and Takashima, A. (2001) *J. Biol. Chem.* **276,** 32293–32299
27. Parbhu, A., Lin, H., Thimm, J., and Lal, R. (2002) *Peptides* **23,** 1265–1270
28. Curtain, C. C., Ali, F., Volitakis, I., Cherny, R. A., Norton, R. S., Beyreuther, K., Barrow, C. J., Masters, C. L., Bush, A. I., and Barnham, K. J. (2001) *J. Biol. Chem.* **276,** 20466–20473
29. Valko, M., Morris, H., and Cronin, M. T. (2005) *Curr. Med. Chem.* **12,** 1161–1208
30. Bush, A. I., Pettingell, W. H., Jr., de Paradis, M., Tanzi, R. E., and Wasco, W. (1994) *J. Biol. Chem.* **269,** 26618–26621
31. Liu, S. T., Howlett, G., and Barrow, C. J. (1999) *Biochemistry* **38,** 9373–9378
32. Miura, T., Suzuki, K., Kohata, N., and Takeuchi, H. (2000) *Biochemistry* **39,** 7024–7031
33. Yang, D. S., McLaurin, J., Qin, K., Westaway, D., and Fraser, P. E. (2000) *Eur. J. Biochem.* **267,** 6692–6698
34. Kozin, S. A., Zirah, S., Rebuffat, S., Hoa, G. H., and Debey, P. (2001) *Biochem. Biophys. Res. Commun.* **285,** 959–964
35. Zirah, S., Rebuffat, S., Kozin, S. A., Debey, P., Fournier, F., Lesage, D., and Tabet, J. C. (2003) *Int. J. Mass Spectrom.* **228,** 999–1016
36. Mekmouche, Y., Coppel, Y., Hochgrafe, K., Guilloreau, L., Talmard, C., Mazarguil, H., and Faller, P. (2005) *Chembiochem.* **6,** 1663–1671
37. Geiger, T., and Clarke, S. (1987) *J. Biol. Chem.* **262,** 785–794
38. Stephenson, R. C., and Clarke, S. (1989) *J. Biol. Chem.* **264,** 6164–6170
39. Roher, A. E., Lowenson, J. D., Clarke, S., Wolkow, C., Wang, R., Cotter, R. J., Reardon, I. M., Zurcher-Neely, H. A., Heinrikson, R. L., Ball, M. J., and Greenberg, B. D. (1993) *J. Biol. Chem.* **268,** 3072–3083
40. Kuo, Y. M., Webster, S., Emmerling, M. R., De Lima, N., and Roher, A. E. (1998) *Biochim. Biophys. Acta* **1406,** 291–298
41. Fabian, H., Szendrei, G. I., Mantsch, H. H., Greenberg, B. D., and Otvos, L., Jr. (1994) *Eur. J. Biochem.* **221,** 959–964
42. Orpiszewski, J., Schormann, N., Kluve-Beckerman, B., Liepnieks, J. J., and Benson, M. D. (2000) *FASEB J.* **14,** 1255–1263
43. Fonseca, M. I., Head, E., Velazquez, P., Cotman, C. W., and Tenner, A. J. (1999) *Exp. Neurol.* **157,** 277–288
44. Frenkel, D., Dewachter, I., Van Leuven, F., and Solomon, B. (2003) *Vaccine* **21,** 1060–1065
45. Chauhan, N. B., and Siegel, G. J. (2005) *Neurosci. Lett.* **375,** 143–147
46. Gelinas, D. S., DaSilva, K., Fenili, D., St George-Hyslop, P., and McLaurin, J. (2004) *Proc. Natl. Acad. Sci. U. S. A.* **101,** Suppl. 2, 14657–14662
47. Zirah, S., Stefanescu, R., Manea, M., Tian, X., Cecal, R., Kozin, S. A., Debey, P., Rebuffat, S., and Przybylski, M. (2004) *Biochem. Biophys. Res. Commun.* **321,** 324–328
48. Wishart, D. S., Sykes, B. D., and Richards, F. M. (1992) *Biochemistry* **31,** 1647–1651
49. Wishart, D. S., and Sykes, B. D. (1994) *J. Biomol. NMR* **4,** 171–180
50. Forman-Kay, J. D., Clore, G. M., and Gronenborn, A. M. (1992) *Biochemistry* **31,** 3442–3452
51. Perez-Canadillas, J. M., Campos-Olivas, R., Lacadena, J., Martinez del Pozo, A., Gavilanes, J. G., Santoro, J., Rico, M., and Bruix, M. (1998) *Biochemistry* **37,** 15865–15876
52. Pardi, A., Billeter, M., and Wuthrich, K. (1984) *J. Mol. Biol.* **180,** 741–751
53. Mazur, A. K. (2001) in *Computational Biochemistry and Biophysics* (Becker, O. M., MacKerell, Jr., A. D., Roux, B., and Watanabe, M., eds) pp. 115–131, Marcel Dekker, Inc., New York
54. Braun, W., and Go, N. (1985) *J. Mol. Biol.* **186,** 611–626
55. Nilges, M., Gronenborn, A. M., Brunger, A. T., and Clore, G. M. (1988) *Protein Eng.* **2,** 27–38
56. Brooks, B. R., Bruccoleri, R. E., Olafson, B. D., States, D. J., Swaminathan, S., and Karplus, M. (1983) *J. Comput. Chem.* **4,** 187–217
57. Cornell, W. D., Cieplak, P., Bayly, C. I., GouldIan, R., Merz, K. M., Ferguson, D. M.,

Spellmeyer, D. C., Fox, T., Caldwell, J. W., and Kollman, P. A. (1995) *J. Am. Chem. Soc.* **117,** 5179–5197
58. Koradi, R., Billeter, M., and Wuthrich, K. (1996) *J. Mol. Graphics* **14,** 51–55, 29–32
59. Bernstein, H. J. (2000) *Trends Biochem. Sci.* **25,** 453–455
60. Laskowski, R. A., MacArthur, M. W., Moss, D. S., and Thornton, J. M. (1993) *J. Appl. Crystallogr.* **26,** 283–291
61. Paranandi, M. V., Guzzetta, A. W., Hancock, W. S., and Aswad, D. W. (1994) *J. Biol. Chem.* **269,** 243–253
62. Wellner, D., Panneerselvam, C., and Horecker, B. L. (1990) *Proc. Natl. Acad. Sci. U. S. A.* **87,** 1947–1949
63. Bodo, B., Rebuffat, S., El Hajji, M., and Davoust, D. (1985) *J. Am. Chem. Soc.* **107,** 6011–6017
64. Wuthrich, K. (1986) *NMR of Proteins and Nucleic Acids*, John Wiley & Sons, Inc., New York
65. Chazin, W. J., Kordel, J., Thulin, E., Hofmann, T., Drakenberg, T., and Forsen, S. (1989) *Biochemistry* **28,** 8646–8653
66. Matsubara, T., Hiura, Y., Kawahito, O., Yasuzawa, M., and Kawashiro, K. (2003) *FEBS Lett.* **555,** 317–321
67. O'Hair, R. J., Bowie, J. H., and Gronert, S. (1992) *Int. J. Mass Spectrom.* **117,** 23–36
68. Huang, X., Atwood, C. S., Moir, R. D., Hartshorn, M. A., Vonsattel, J. P., Tanzi, R. E., and Bush, A. I. (1997) *J. Biol. Chem.* **272,** 26464–26470
69. Hou, L., Shao, H., Zhang, Y., Li, H., Menon, N. K., Neuhaus, E. B., Brewer, J. M., Byeon, I. J., Ray, D. G., Vitek, M. P., Iwashita, T., Makula, R. A., Przybyla, A. B., and Zagorski, M. G. (2004) *J. Am. Chem. Soc.* **126,** 1992–2005
70. Shimizu, T., Watanabe, A., Ogawara, M., Mori, H., and Shirasawa, T. (2000) *Arch. Biochem. Biophys.* **381,** 225–234
71. Saido, T. C., Yamao-Harigaya, W., Iwatsubo, T., and Kawashima, S. (1996) *Neurosci. Lett.* **215,** 173–176